

RESEARCH ARTICLE

Espin overexpression causes stereocilia defects and provides an anti-capping effect on actin polymerization

Lili Zheng¹ | Stephen A. Adam¹ | Jaime García-Anoveros^{2,3} | Brian J. Mitchell¹ | James R. Bartles^{1,3,#}

¹Department of Cell and Developmental Biology, Northwestern University, Feinberg School of Medicine, Chicago, Illinois, USA

²Department of Anesthesiology Neurology and Neuroscience, Northwestern University, Feinberg School of Medicine, Chicago, Illinois, USA

³Hugh Knowles Center for Clinical and Basic Science in Hearing and its Disorders, Northwestern University, Feinberg School of Medicine, Chicago, Illinois, USA

Correspondence

James R. Bartles, Department of Cell and Developmental Biology Northwestern University, Feinberg School of Medicine, 303. E. Chicago Ave, Chicago, Illinois, 60611 USA. Email: j-bartles@northwestern.edu

Brian J. Mitchell, Northwestern University, Department of Cell and Developmental Biology, 303. E. Chicago Ave, Chicago, Illinois 60611 USA. Email: brian-mitchell@northwestern.edu

Funding information

National Institute of General Medical Sciences; National Institutes of Health

Abstract

Stereocilia are actin-based projections of hair cells that are arranged in a step like array, in rows of increasing height, and that constitute the mechanosensory organelle used for the senses of hearing and balance. In order to function properly, stereocilia must attain precise sizes in different hair cell types and must coordinately form distinct rows with varying lengths. Espins are actin-bundling proteins that have a well-characterized role in stereocilia formation; loss of function mutations in Espin result in shorter stereocilia and deafness in the *jerker* mouse. Here we describe the generation of an Espin overexpressing transgenic mouse line that results in longer first row stereocilia and discoordination of second-row stereocilia length. Furthermore, Espin overexpression results in the misregulation of other stereocilia factors including GNAI3, GPSM2, EPS8, WHRN, and MYO15A, revealing that GNAI3 and GPSM2 are dispensable for stereocilia overgrowth. Finally, using an in vitro actin polymerization assay we show that espin provides an anti-capping function that requires both the G-actin binding WH2 domain as well as either the C-terminal F-actin binding domain or the internal xAB actin-binding domain. Our results provide a novel function for Espins at the barbed ends of actin filaments distinct from its previous known function of actin bundling that may account for their effects on stereocilia growth.

KEYWORDS

actin, espin, hair cell, stereocilia

1 | INTRODUCTION

Staircase-like arrays of stereocilia on inner ear hair cells serve as detectors for our hearing and our vestibular sense. An estimated 37.5 million Americans have hearing impairment (Blackwell, Lucas, & Clarke, 2014), and an estimated 35% of Americans have experienced a vestibular disorder (Agrawal, Carey, Della Santina, Schubert, & Minor, 2009). Genetic mutations (Drummond, 2012; Richardson, de

Monvel, & Petit, 2011) and proteomics (Shin et al., 2013) have helped to identify molecules involved in stereocilia morphogenesis and function.

Sensing by inner-ear hair cells relies on staircase-like arrays of finger-like projections known as stereocilia. The deflection of stereocilia caused by sound and movement initiates a type of mechanosensation that depends on precise variations in stereocilium length. Stereocilia range in size according to hair cell location within the cochlea or vestibular epithelia, and in each hair cell according to the row they occupy within the bundle (Richardson

Deceased

et al., 2011; Schwander, Kachar, & Müller, 2010; Vollrath, Kwan, & Corey, 2007).

At their core, stereocilia contain a parallel actin bundle, which is thought to act as a scaffold that determines their location, dimensions and mechanical properties. Hair cell stereocilia grow to precise dimensions from microvillus-like precursors in coordination with their parallel actin bundle scaffold (Tilney & DeRosier, 1986). Parallel actin bundles are then held together by actin-bundling proteins (Bartles, 2000). Stereocilia contain three classes of actin-bundling protein: espins, fascin, and fimbrin/plastins (Krey et al., 2016; Perrin et al., 2013; Sekerková et al., 2004). We originally discovered espin as a novel ~100 kDa actin-binding protein enriched in the actin bundle-rich plaque of Sertoli cell junctions (Bartles, Wierda, & Zheng, 1996). The espin gene encodes multiple size variant isoforms and a small espin isoform of ~30 kDa was enriched in the brush border microvilli of intestine and kidney (Bartles, Zheng, Li, Wierda, & Chen, 1998).

Espins are enriched in hair cell stereocilia and are the target of the *jerker* mutation in mice (Zheng et al., 2000). *Jerker* is a spontaneous recessive mutation that causes deafness and vestibular dysfunction (circling) in mice (Bock & Steel, 1983; Grüneberg, Burnett, & Snell, 1941). The *jerker* mutation is a single nucleotide deletion, which causes a frameshift mutation in all espin isoforms and blocks the accumulation of espin proteins in homozygous *jerker* mice (Zheng et al., 2000). Revised estimates of espin stoichiometry obtained by targeted proteomics are ~15,000 molecules per utricular stereocilium, similar to the levels of fascin 2 cross-linker (Krey et al., 2016). The lack of espin proteins in homozygous *jerker* mice results in stereocilia that are abnormally short, thin, and unstable (Sekerková, Richter, & Bartles, 2011). These stereocilia defects are more severe than those caused by inactivation of fascin 2 by the R109H mutation (Krey et al., 2016; Perrin et al., 2013) or by knockout of plastin 1 (Krey et al., 2016).

Here we examine the effect of espin over-expression on hair cell stereocilia morphogenesis. We find that an approximately two-fold increase in espin levels leads to enlarged row 1 stereocilia on hair cells in the cochlea, utricle and cristae. Along with these changes in stereocilia morphology, we also find that several proteins involved in stereocilia function are mislocalized, which suggests that two proteins that are normally required for stereocilia growth (GPSM2 and GNAI3) are actually dispensable in espin overexpressing hair cells. Finally, in vitro actin polymerization experiments reveal a novel anti-capping activity for espins in stereocilia that is consistent with, and can explain, their enlargement due to excess levels of espin.

2 | RESULTS

Here, we examine what happens when espins are over-expressed in mice. Espin BAC-transgenic mice were prepared by pronuclear microinjection of BAC RP23-284C20 at the Northwestern University Transgenic and Targeted Mutagenesis Laboratory. The BAC, which carries an 81,620-bp fragment of mouse chromosome 4 in the pBACe3.6 vector (GenBank Accession number AL772240.7), was

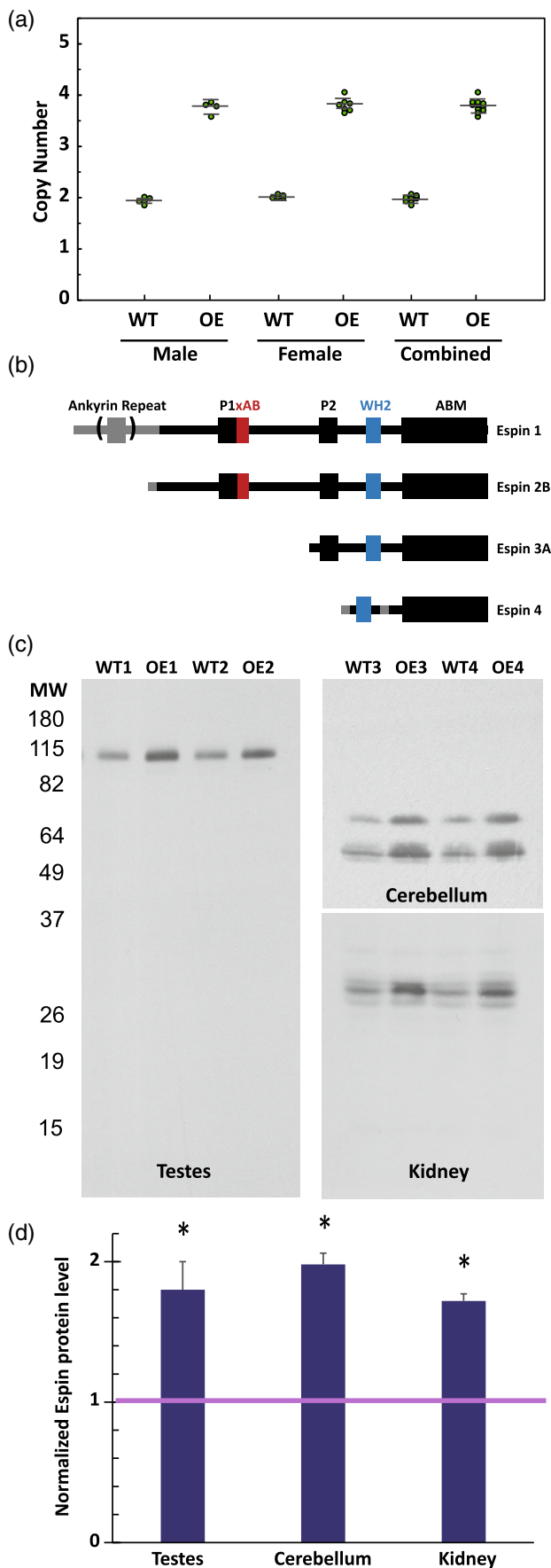
purchased from the BACPAC Resource Center (BACPAC Genomics, Richmond, CA). The BAC contains the entire 32,040 bp mouse *espin* gene (*Espn*) and includes ~38 kb of upstream flanking sequence.

Also included in the fragment are two smaller genes, *Hes2* and *Tnfrsf25*, the 3' half of *Plekhh5* and 242 bp at the 5' end of *Acot7*. *Hes2* encodes a basic helix-loop-helix transcriptional repressor in the Hes family of mammalian *hairly* and *enhancer of split* orthologs. On Northern blots, *Hes2* mRNA was detected in multiple tissues of late-embryonic and adult rats (Kageyama, Shimojo, & Imayoshi, 2015). Although different Hes family members have been shown to maintain stem cell populations and establish tissue boundaries (Kageyama et al., 2015), the function of *Hes2* is currently unknown. *Tnfrsf25*, also known as death receptor 3, is expressed in subsets of T and B lymphocytes (Schreiber & Podack, 2013; Schreiber, Wolf, Boder, Gonzalez, & Podack, 2012). Although *Tnfrsf25* can mediate apoptosis, it most often responds to its TNF-like protein 1A ligand to promote gene activation leading to enhanced cell survival and inflammation (Collins et al., 2015; Fang et al., 2015). HES2 and TNFRSF25 have not been reported to affect hair cells, neither protein has been detected in hair bundle preparations (Krey, Wilmarth, David, & Barr-Gillespie, 2017), and neither gene expresses its mRNA in hair cells at detectable or physiologically-relevant levels (Orvis et al., 2021; Schefter, Shen, Corey, & Chen, 2015; Wiwatpanit et al., 2018). Hence, any effects of this BAC transgene on hair cells are most likely due to over-expression of espins.

Mice positive for the transgene were identified by PCR using primers for the *chloramphenicol acetyltransferase* gene in the pBACe3.6 vector. From two rounds of microinjection, we obtained 5 positive founder mice, but only one gave stable expression of the transgene over two subsequent generations. To minimize the effects of difference in genetic background and age-related hearing loss, we backcrossed that line into the CBA/CaJ inbred strain for 26 generations, so it is now considered CBA/CaJ congenic: CBACa.Cg-Tg (RP23-284C20)/Jbart. In the experiments that follow, the espin-BAC transgenic mice are heterozygous for the transgene.

Taqman Copy Number qPCR assays showed that in both males and females there were ~3.8 copies of the *Espn* gene in the genomic DNA of our espin-BAC transgenic mice relative to 2.0 copies in the wild-type (Figure 1a). The espin-BAC transgenic mice displayed no overt behavioral phenotype. However, they did show over-expression of the expected espin isoform(s) in multiple mouse tissues. There are 4 prominent isoforms of espin (Figure 1b) and we have previously characterized their tissue distribution and found a ~91 kDa isoform in testis (espin 1), ~55 and ~65 kDa in the cerebellum (espins 2A and 2B) and ~28 kDa triplet in kidneys (espin 4). Estimates of espin isoform levels from western blot comparisons of postnatal day 60 (P60) mice showed that the espin-BAC transgenic mice contain 1.7–2.0 times wild-type levels for each of these tissues/isoforms (Figure 1c-d). We will therefore now refer to these mice as espin overexpressing (OE).

The espin-OE mice did not show gross anatomical alterations in their inner ears, but they did show a striking enlargement of stereocilia. At P60, enlarged stereocilia were detected on hair cells in the



cochlea, utricle and cristae. The elongation of stereocilia was easy to see in 3D confocal reconstructions (Figure 2a,b). For example, at mid-cochlea, the length of the tallest-row stereocilia on inner hair cells increased ~ 1.5 -fold in length, from $4.8 \pm 0.6 \mu\text{m}$ to $7.1 \pm 0.8 \mu\text{m}$ (mean \pm SD; $n = 140$ stereocilia; t -test, $p < 0.0001$) (Figure 2c-e). Similarly, the length of tallest row stereocilia from outer hair cells increased from $1.9 \pm 0.4 \mu\text{m}$ to $3.6 \pm 0.6 \mu\text{m}$ (mean SD; $n = 120$ stereocilia; t -test, $p < 0.0001$) (Figure 2f-h).

Similar to the cochlea we found that first row stereocilia of the extrastriolar region of the utricle increased ~ 1.6 -fold, from $\sim 13 \mu\text{m}$ to $\sim 20 \mu\text{m}$ (Figure 3a,b). This result was confirmed using scanning electron microscopy (Figure 3c,d). Furthermore, in contrast to the first row stereocilia, the additional rows all appear considerably stunted (Figure 3c,d). Interestingly, first row stereocilia in the *espin*-OE mice were not only longer; they were also wider. We used structured illumination microscopy (SIM) to measure the width of isolated utricular stereocilia at sub-diffraction resolution (Figure 3e-g). Utricules were plated with stereocilia pointing down on poly-lysine-coated coverslips, fixed, washed with 0.5% Triton X-100 and labeled with Texas Red-phalloidin to stain actin filaments. SIM analysis showed that the width in the middle of the stereocilia increased from $191 \pm 26 \text{ nm}$ in wild-type mice to $257 \pm 27 \text{ nm}$ in *espin*-OE mice whereas at the tip the width increased from $229 \pm 27 \text{ nm}$ to $321 \pm 32 \text{ nm}$ (Figure 3g; $n = 109$ stereocilia; t -test, $p < 0.0001$).

Stereocilia size is known to be modulated by a number of factors. The G protein signaling modulator p2-inhibitory G protein alpha (GPSM2-GNAI3) pathway affects the shape and polarity of the array and involves the participation of myosin 15A (MYO15A), the actin regulator capping protein EPS8, and the PDZ containing scaffold protein whirlin (WHRN) in the hair cell (Fang et al., 2015; Mathur et al., 2015; Mauriac et al., 2017; Tadenev et al., 2019). We therefore determined if *espin*-OE had an effect on any of these key regulators. In WT animals antibody staining of GPSM2 and GNAI3 reveals strong localization to the tips of row 1 stereocilia at P10 (Tadenev et al., 2019) (Figure 4a,b). In striking contrast, *espin*-OE animals had a near complete loss of these proteins from the stereocilia. This result is somewhat paradoxical as genetic depletion of GPSM2 or GNAI3 has previously been shown to result in short stunted stereocilia rather than the elongated ones observed with *espin*-OE. This result suggested that other factors may be altered underlying the observed phenotypes. We next visualized the capping protein EPS8 and found that in P10 WT animals EPS8 is primarily localized to the tips of row 1 stereocilia, whereas in *espin*-OE animals it is often observed not

FIGURE 1 Validation of Espin over-expression. (a) TaqMan real-time PCR based copy number assay for wild type (WT) and *espin* OE (OE). Data is presented as both male (n of 4 WT and 4 OE), female (n of 4 WT and 7OE) and combined. (b) Domain architecture for the 4 main isoforms of the *espin* gene. (c) Western blot analysis of *espin* protein levels in the testes (Espin 1, 2 representative animals), in the cerebellum (*espin* 2, 2 representative animals), and in the kidney (*espin* 4, 2 representative animals). (d) Normalized quantification of *espin* levels ($n = 6$; error bars represent S.D., t -test $*p < 0.05$)

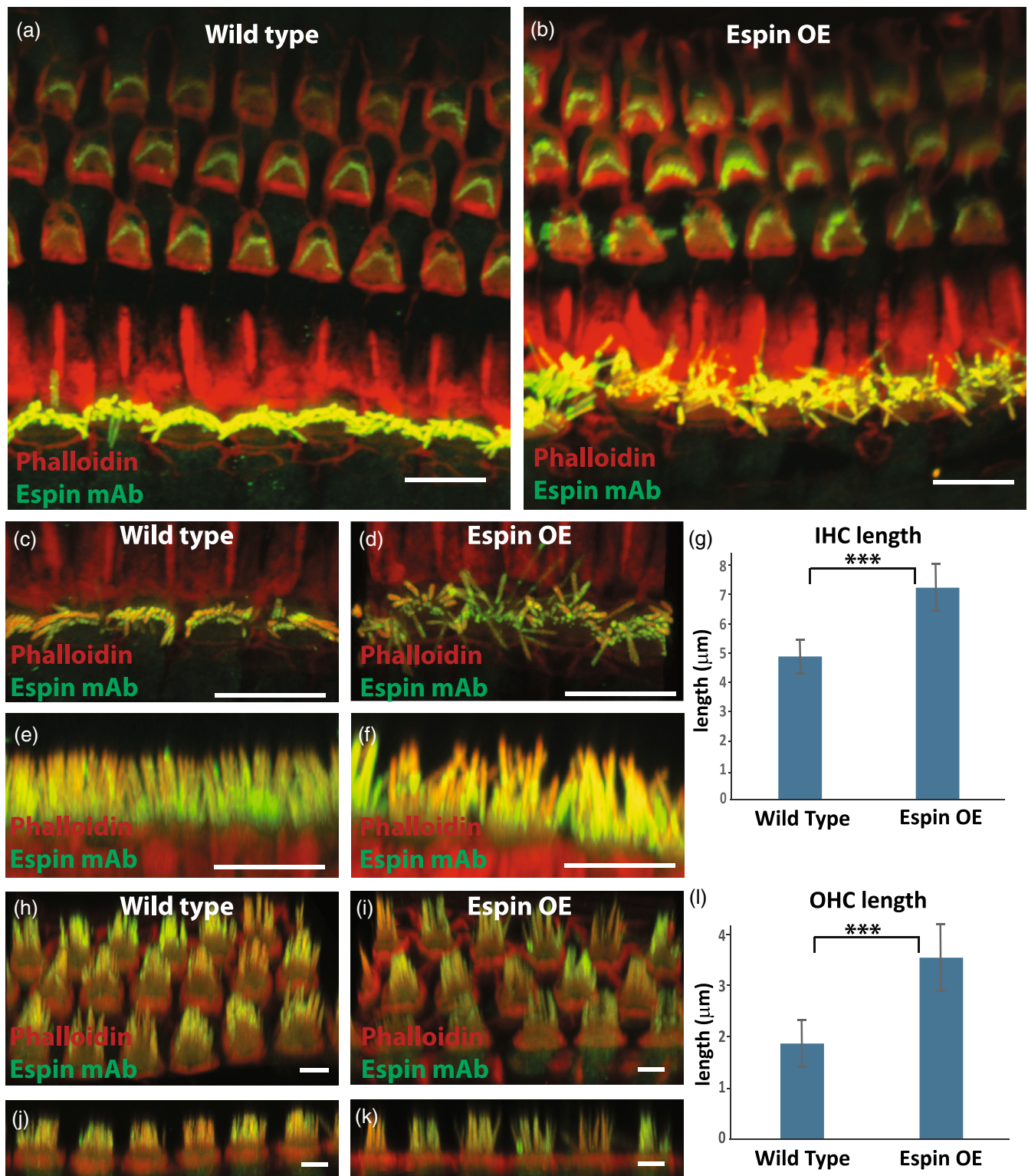


FIGURE 2 Espin-OE alters cochlear stereocilia length. (a-b) Antibody staining of espin (green) together with phalloidin (red) of wild type (a) and espin-OE (b) cochlea depicting a grossly normal organization of outer hair cells and a mild disorganization of inner hair cells. (c-g) Top and side projection of wild type (c, e) and espin-OE (d, f) inner hair cells together with the quantification of tallest row stereocilia length (g, $n = 140$ stereocilia from ≤ 8 cochlea per condition). (h-l) Tilted projection and side projection of wild type (h, j) and espin OE (i, k), together with quantification of tallest row stereocilia length (l, $n = 120$ stereocilia from ≤ 9 cochlea per condition). Statistics performed were Student's *t*-test and *** represents a *p* value < 0.0001 . Scale bars are $5 \mu\text{m}$

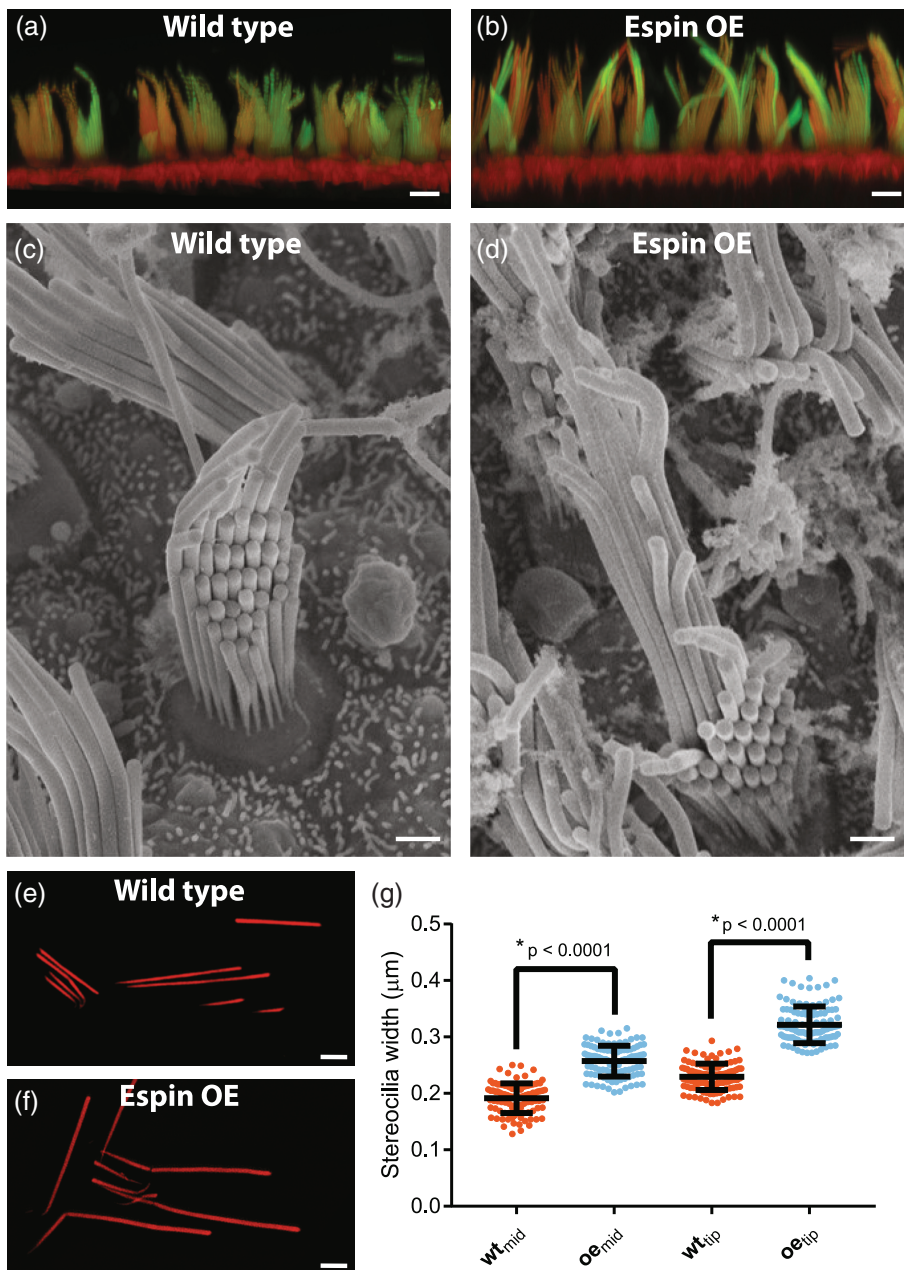


FIGURE 3 Espin-OE alters utricle stereocilia length. (a-b) Antibody staining of espin (green) together with phalloidin (red) of wild type (a) and espin-OE (b) utricle hair cells. (c-d) TEM micrographs of wild type (c) and espin-OE (d) utricle hair cells. (e-g) Structured illumination microscopy of isolated utricle stereocilia from wild type (e) and espin-OE (f) cells. (g) Quantification of stereocilia width measured at both in the middle and at the tip of the isolated stereocilia ($n = 105$ stereocilia each condition). Scale bar is $5 \mu\text{m}$ in a-b and $1 \mu\text{m}$ in c-f

only at the tips of row 1 stereocilia but also at the tips of the other shorter rows of stereocilia. (Figure 4c). Similarly, the scaffold protein WHRN localization is also expanded beyond the tips of row 1 and could be found sporadically at tips in other rows. Finally, MYO15A is known to be important for trafficking other proteins in stereocilia and has well-characterized functional significance. There are two isoforms of MYO15A, a shorter version that is essential for proper stereocilia formation and a longer version that is expressed later and is essential for stereocilia maintenance (Fang, Adkins, Deyev, & Podack, 2008). The MYO15A antibody, PB888 only recognizes the longer isoform and at P10 is primarily localized to the tips of shorter (non-row 1) stereocilia (Figure 4e). While the localization of MYO15A appears quite similar in the espin-OE mice, the concentration appears substantially increased (Figure 4e). In contrast, the MYO15A antibody PB48

recognizes both the long and short isoforms and is enriched at the tips of first row stereocilia, even in animals deficient for the shorter isoform, indicating that it is primarily recognizing the long isoform. Interestingly, in espin-OE animals stained with PB48 we see an enrichment at the tips of non-row 1 stereocilia (Figure 4f) and, taken together with the results from PB888, suggests that the long MYO15A is dramatically altered in espin-OE mice.

While espins are well characterized for their role in actin bundling, our previous work has suggested that they may have a distinct and independent function at the tips of stereocilia. First, using a pan-espin antibody, we have shown localization along the entire length of stereocilia, whereas using an antibody specific for the longer isoforms (espin1 and 2) we see enrichment at the distal tips (Zheng, Beeler, & Bartles, 2014). The longer isoforms of espin contain a second F-actin

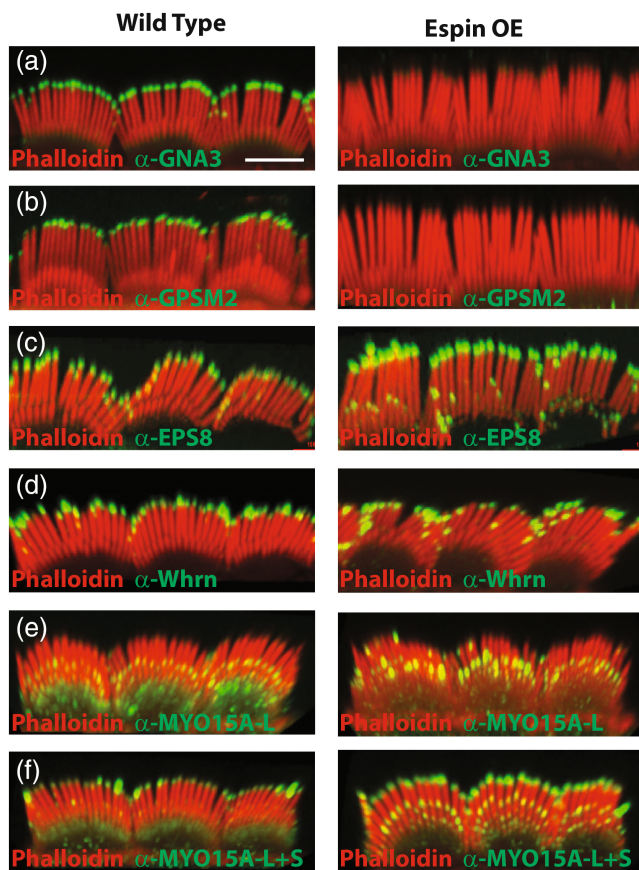


FIGURE 4 Espin-OE drives mis-localization of stereocilia proteins. (a-f) Antibody staining of P10 cochlea from wild type animals on the left and espin-OE animals on the right stained with phalloidin (red) and antibodies to GNAI3 (a), GPSM2 (b), EPS8 (c), WHRN (d), MYO15A-L (e), and MYO15A-L + S (f) in green. Images are representative of $n > 3$ animals. Scale bar is 5 μm

binding domain (xAB; Fig 1b) which can be autoinhibited by the ankyrin repeats found in espin 1 but not espin 2. Importantly, in espin 2B-induced elongated microvilli we have shown that there is no recovery (of GFP) after photo-bleaching with the wild-type protein fused to GFP, but that there is significant recovery from the barbed end in cells expressing an espin 2B with a mutated, actin binding deficient, xAB (L145A). This result suggested to us that espin has a distinct barbed end-specific function that is regulated via the xAB domain. To address this possibility, we turned to an *in vitro* pyrene-actin polymerization assay (Zheng et al., 2014). Using GST purified proteins, we found that the polymerization of actin is slightly decreased in the presence of espin 2B likely due to its bundling capacity (Figure 5a). In contrast actin polymerization is essentially eliminated in the presence of Capping Protein (CP), a known negative regulator of actin polymerization. Importantly, the effect of CP on actin polymerization is blocked by the addition of espin 2B in a dose dependent manner (Figure 5a) suggesting that espin has an anti-capping function distinct from its actin bundling function. As only the long isoforms of espin specifically localize to the tips of stereocilia, we

set out to determine the domain requirements for the anti-capping function. We have identified critical residues that modulate the function of distinct domains within espin. For example, we previously published the xAB domain mutation L145A leads to a loss of F-actin binding and nuclear actin bundling (Zheng et al., 2014). Similarly, the 116 AA C-terminal actin binding motif (ABM) contains 3, 12 AA Tryptophan (W) containing pseudo-repeats (Figure S1a). Mutation of these W's to Alanines (3 W) leads to a considerable loss of F-actin binding, actin bundling and the ability to generate ectopic microvilli (Figure S1b-d). Finally, WH2 domains are known modulators of actin function. We have previously shown that the WH2 domain of espin binds monomeric G-actin and inhibits the actin polymerization rate in a dose dependent manner (Zheng et al., 2014). Furthermore, the WH2 domain facilitates actin bundling and mutations of the 3 WH2 core leucine's into alanine's (3LA) block its bundling function (Loomis et al., 2006).

We used these 3 mutants to assess the ability of espin 2B to block CP function. Espin 2B-3LA caused a slight increase in actin polymerization over WT espin 2B consistent with its loss of bundling function (Figure 5c). However, in contrast to WT protein the espin 2B-3LA failed to considerably block the CP inhibition of actin polymerization suggesting that the WH2 domain is important for this function (Figure 5c). Next, we addressed the function of the xAB domain. Interestingly, the espin 2B-L145A mutant maintained its potent anti-CP function, completely blocking CP inhibition of polymerization (Figure 5d). Similarly, mutations to the ABM domain espin2B-3 W also completely block CP inhibition (Figure 5e). Mutations of both the ABM and WH2 (espin2B-3LA-3 W) lost the ability to block CP function confirming the importance of the WH2 domain (Figure 5e). Finally, mutations of the xAB and the ABM lost the ability to efficiently block CP inhibition. This result indicates that in addition to the G-actin binding WH2 domain, there is a requirement for F-actin binding that can be provided by either the xAB or the ABM.

3 | DISCUSSION

The present work, together with previous work utilizing both homozygote and heterozygote loss of function mutations in the mouse *espn* gene (*Jerker* mouse) indicates that gene dosage/protein levels of *Espin* represent a critical aspect of regulating stereocilia growth (Sekerková et al., 2011). Specifically, homozygous *Jerker* mice have the shortest and thinnest stereocilia, whereas heterozygous *Jerker* mice have intermediate length and width followed by wild type and ultimately our overexpression mice result in larger and wider stereocilia. Because gene copy number in these animals was estimated close to four (the wild type having the expected two alleles) and the levels of *ESPN* protein in overexpressing heterozygotes nearly doubles that of wild types, we conclude that two copies of the espin transgene were inserted, doubling the gene dosage of wild types. These results reveal that *espin* gene dosage and controlled expression levels are critical for achieving the precise size of stereocilia. This has implications for gene

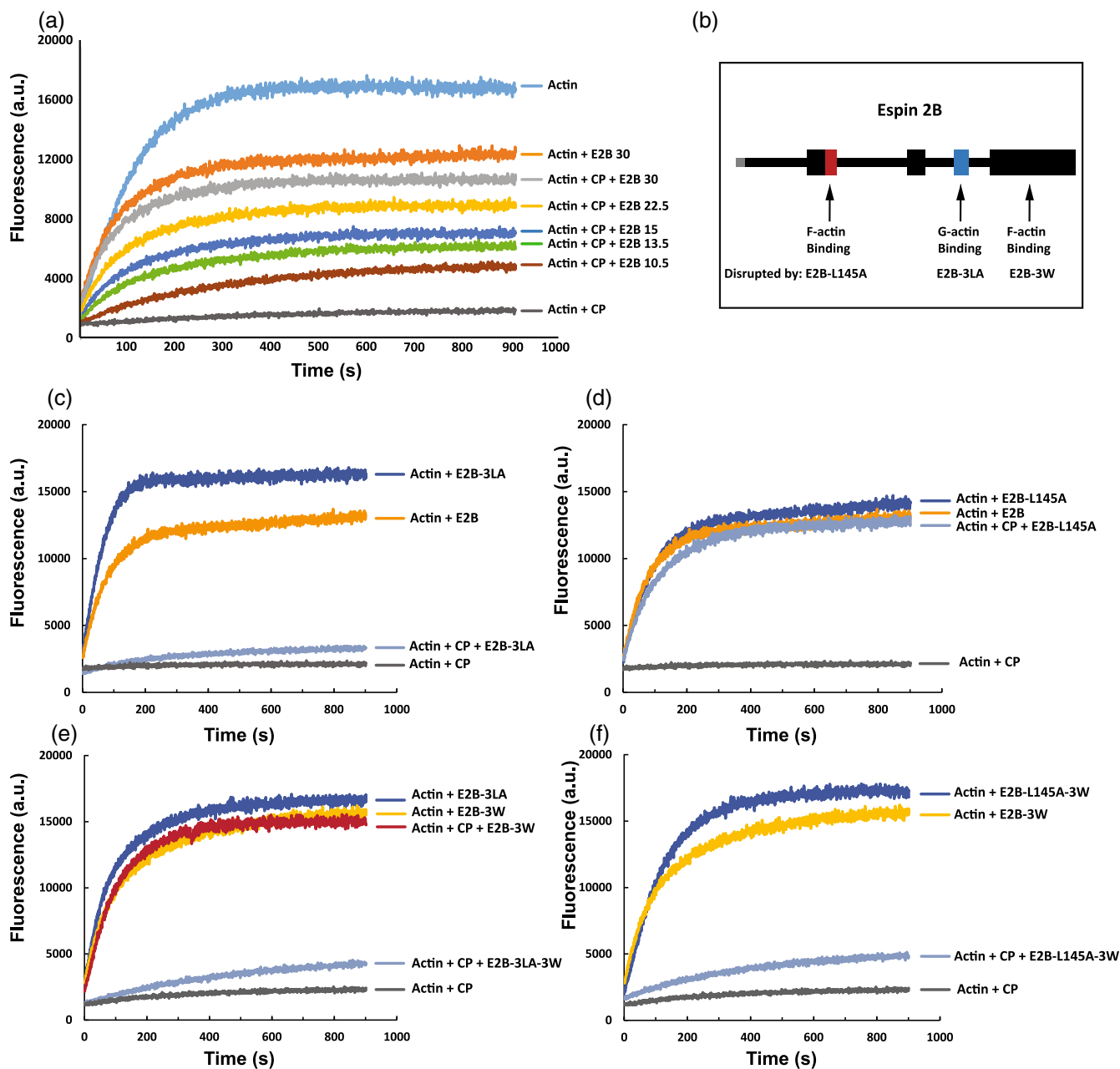


FIGURE 5 Espin has anti-capping function. (a) Spectrofluorimetric pyrene-Actin polymerization assay examining the block of polymerization with the addition of capping protein (CP) and an increasing anti-capping effect with increasing amounts (μg) of wild type espin2B (E2B). (b) Graphical representation of espin2B Actin binding domains as well as the mutations that disrupt each domain, with the E2B-L145A mutation disrupting the xAb site, the E2B-3LA disrupting the WH2 site and E2B-3 W disrupting the ABM site (See text and Figure S1). (c-f) Spectrofluorimetric pyrene-Actin polymerization assessing the ability of E2B-3LA (c), E2B-L145A (d), E2B-3 W and E2B-3 W + 3LA (e), and E2B-3 W + L145A (f) to provide anti-capping effect against CP

therapy approaches to treat human deafness caused by mutations in *espin*, many of which are inherited in a recessive manner (DFNB36 [Boulouiz et al., 2008; Naz et al., 2004]), although some missense mutations display dominant inheritance (Donaudy et al., 2006). In general, the favored strategy for restoring hearing caused by recessive, loss-of-function mutations is simply to express a copy of the gene under a generic promoter, something that is becoming feasible with AAV vectors targeting hair cells. However, in the case of *Espn*,

transgene expression is likely to exceed the wild-type levels and result in an opposite but still harmful defect in hair cells. Instead, the recommended approach for DFNB36 patients would be gene editing to correct the mutations in the endogenous *Espn* alleles.

The staircase arrangement of hair cell stereociliary bundles begins to develop as stereocilia from the first row grow above those of the other rows. This elongation is accompanied by an accumulation of several proteins at the tips of row one stereocilia: a short isoform of

MYO15A, the actin regulator capping protein EPS8, and the PDZ containing scaffold protein WHRN, which form a protein complex to which GPSM2 and GNAI3 are incorporated (Mauriac et al., 2017; Tadenev et al., 2019). These five proteins seem to be required for the elongation of row 1 stereocilia, as in mutants for each of them all stereocilia remain short (Holme, Kiernan, Brown, & Steel, 2002; Mauriac et al., 2017; Probst et al., 1998; Tadenev et al., 2019; Zampini et al., 2011). In the *espin*-OE mice, row 1 stereocilia grow excessively, and indeed we find that their tips contain the short isoform of MYO15A, EPS8, and WHRN. However, and unexpectedly, the tips of these overgrowing row 1 stereocilia lack (at least at the usual detectable levels) both GPSM2 and GNAI3. Hence, although the G protein signaling modulator p2-inhibitory G protein alpha pathway may be normally involved in stereocilia elongation, it does not appear to be essential for it to occur. Elucidating the mechanisms by which GPSM2 and GNAI3 promote row 1 stereocilia elongation must take into consideration that both proteins appear to be dispensable. Whatever their function is, it seems that it can be bypassed by a doubling in the levels of *espin*.

Our study reveals a potential mechanism by which excess *espin* protein may lead to stereocilia overgrowth, which is their newly found anti-capping activity at the barb ends of actin filaments. *Espsins* are known as actin-bundling proteins, and their localization along the actin-rich stereocilia is consistent with such a role. However, the longer isoforms of *espin* (1 and 2B) localize at the tips of stereocilia (Zheng et al., 2014), and as we have seen one of these isoforms (*espin* 2B) does overcome the capping of actin filaments, permitting their continued polymerization, in a concentration-dependent manner. This anti-capping activity would explain why doubling the amount of *espin* would promote excess actin-bundle polymerization and hence stereocilia growth. Why this happens only in row 1 stereocilia remains to be explained.

4 | MATERIALS AND METHODS

All animal work was performed ethically according to US National Research Council's Guide for the Care and Use of Laboratory Animals using protocols approved by the Northwestern IACUC.

4.1 | Confocal microscopy

Dissected cochlear were fixed with 2% (w/v) paraformaldehyde in PBS pH 7.4 for 1HR then processed in the same buffer containing 0.01% (w/v) saponin. Samples were quenched with 0.25% (w/v) ammonium chloride/saponin/PBS for 5 min, two times. Permeabilized for 5 min with ice-cold 0.4% (v/v) Triton X-100/PBS, and quenched 3–5 min. Samples were blocked in 5% (v/v) goat serum in saponin/PBS for 15 min before the overnight incubation with primary antibody at 40C. The second day, the samples were washed three times with saponin/PBS, then incubated for 2.5 hr in secondary antibodies at room temperature. Samples were imaged in the

Northwestern CAM facility on a Nikon A1R microscope using a 100X objective (N.A. 1.45). Confocal stacks were generated and quantifications were performed on 3D reconstructions using Nikon NIS software.

Antibodies used:

1. Anti-GPSM2 (Sigma Cat No: HPA007327) 1:50, Goat anti-rabbit 488 1:100 (Jackson ImmunoResearch Cat #: 111-545-144)
2. Anti-GNAI3 (Sigma Cat No:G4040) 1:400; Donkey anti-rabbit 488 1:100 (Jackson ImmunoResearch Cat #: 711-546-152)
3. Anti-EPS8 (BD biosciences) 1:180; Donkey anti-mouse 488 1:100 (Jackson ImmunoResearch Cat #: 715-546-151)
4. Anti-WHRN 1:500 (from Jun Yang,[Mathur et al., 2015]); Goat anti-rabbit 488 1:100 (Jackson ImmunoResearch Cat #: 111-545-144)
5. Anti MYO15A-S (PB888; from Jonathan Bird, [Fang et al., 2015]) 1:250; Donkey anti-rabbit 488 1:100 (Cat #: 711-546-152)
6. Anti MYO15A-L (PB48; from Jonathan Bird, [Fang et al., 2015]) 1:200; Donkey anti-rabbit 488 1:100 (Jackson ImmunoResearch Cat #: 711-546-152)

In addition to the secondary antibodies, we add Texas Red-phalloidin (Invitrogen Cat No T7471) 1:80.

4.2 | Structured illumination microscopy

Utricles were dissected and placed with stereocilia pointing down on poly-lysine-coated coverslips and fixed in 4% paraformaldehyde in PBS for 1 hr at room temperature. Unreacted formaldehyde was quenched with 0.25% NH₄CL/PBS for 5 min with one buffer change. The coverslips were then incubated for 4 mins in ice cold 0.5% Triton X-100 in PBS and blocked in 0.4% BSA/PBS for 10–15 mins at room temperature. Texas Red-phalloidin was diluted in 5% non-immune goat serum in PBS and incubated with the coverslips 15 min 37°C. The coverslips were then washed three times with PBS. Imaging was performed on a Nikon N-SIM super resolution microscope with a 100X (N.A. 1.35) Objective.

4.3 | Scanning electron microscopy

Tissues for SEM were prepared as described in (Sekerková et al., 2011) Dissected tissues were fixed with 2.5% glutaraldehyde in the presence of 2 mM CaCl₂, processed using osmium-thiocarbonylhydrazide, critical-point dried, and examined without additional coating in the Hitachi S-4800 field-emission scanning electron microscope in the EPIC Facility at the NUANCE Center.

4.4 | Reagents

All chemicals were from Sigma-Aldrich (St Louis, MO).

Recombinant protein expression and purification.

Recombinant protein expression was carried out essentially as described in (Zheng, Anderson, Miller, Cheatham, & Dallos, 2009). Briefly, recombinant rat espin 2B, formerly known as rat Purkinje cell isoform 1 (GenBank Accession Number [AAO50330](#)), was produced in *Escherichia coli* BL21 Star (DE3) (Life Technologies, Grand Island, NY). Mutations were introduced by PCR or restriction enzyme digestion and checked by DNA sequence analysis. GST fusion proteins were expressed using the pGEX-4 T-2 vector and purified using glutathione-Sepharose 4B (GE Healthcare, Piscataway, NJ) in phosphate-buffered saline, 1 mM dithiothreitol, 1 mM NaN₃, pH 7.4, with elution by 10 mM glutathione. Espin constructs with an N-terminal His-tag were expressed using the ProEX HTa or HTb vector (Life Technologies) and purified using Ni-NTA agarose beads (Qiagen, Valencia, CA) under non-denaturing conditions. Briefly, bacterial extracts prepared in 50 mM Tris-HCl, 10% (v/v) glycerol, 10 mM 2-mercaptoethanol, pH 8.5, were clarified by centrifugation for 30 min at 150,000g. Bead washes contained 20 mM Tris-HCl, 0.1 M KCl, 20 mM imidazole, 12.5 mM 2-mercaptoethanol, 10% (v/v) glycerol, pH 8.5. For His-tagged espins, one intermediate wash step included 1.5 M NaCl, and another included 0.1% (v/v) Triton X-100. For His-tagged human ankyrin repeat domain, 1.0 M KCl was substituted for the 1.5 M NaCl wash, and the Triton X-100 wash was excluded. Elution buffer included 200 mM imidazole. Freshly isolated recombinant proteins were dialyzed overnight into assay buffer and clarified by centrifugation at 150,000 g for 60 min at 4°C before use.

4.5 | Actin filament binding

Purified GST fusion proteins were incubated with preformed filaments of rabbit skeletal muscle actin (AKL99; >99% pure, Cytoskeleton, Denver, CO) (0.4 mg/ml actin) for 60 min at 37°C in 10 mM HEPES, 0.1 M KCl, 1 mM dithiothreitol, 0.5 mM ATP, 1 mM MgCl₂, 1 mM NaN₃, pH 7.4. Pellet and supernatant fractions obtained from centrifugation at 150,000 g for 60 min at 4°C were analyzed in Coomassie-Blue-stained SDS gels.

4.6 | Actin polymerization

Actin polymerization was assayed at 22°C by fluorescence using 5 μM actin with 4% pyrene-actin (Cytoskeleton) (365 nm excitation, 407 nm emission). The inhibition of actin polymerization by GST fusion proteins was examined in the wells of FLUOTRAC 200 96-well, flat-bottom, medium-binding polystyrene microplates (Greiner Bio-One, Monroe, NC) using a Safire² plate reader (Tecan, Männedorf, Switzerland) (Neidt, Skau, & Kovar, 2008). Monomeric actin (10 μM) in 5 mM Tris-HCl, 0.2 mM CaCl₂, 0.2 mM ATP, 0.5 mM dithiothreitol, pH 8.0, was converted to the Mg²⁺ form by adding one-tenth volume of 2 mM EGTA, 0.5 mM MgCl₂, 5 mM Tris-HCl, pH 7.4. After 2 min, an equal volume of purified GST construct was added in 10 mM imidazole-HCl, 0.1 M KCl, 1.6 mM EGTA, 0.5 mM dithiothreitol,

pH 7.4. The slope of the curve from 50 to 200 s was used to compare polymerization rates. Reactions examining His-tagged espin constructs substituted HEPES for imidazole and were performed in a quartz microcuvette in a PC1 spectrofluorimeter (ISS, Champaign, IL).

4.7 | Actin bundling

Actin (1 mg) and 40 μg of rhodamine-rabbit skeletal muscle actin (Cytoskeleton) were hydrated together in 5 mM Tris-HCl, 0.2 mM CaCl₂, 0.2 mM ATP, 0.5 mM dithiothreitol, pH 8.0, overnight and centrifuged at 150,000 g for 20 min at 4°C. In rapid succession, supernatant was diluted to an actin concentration of 5 μM in 10 mM HEPES, 0.1 M KCl, 1 mM dithiothreitol, 3 mM NaN₃, pH 7.4, containing 2 mM MgCl₂ and 1 mM ATP, and an equal volume of 0.25 μM purified His-tagged espin construct in the same buffer minus ATP and MgCl₂ was added. Samples were mixed and incubated for 60 min at 37°C with gentle agitation at intervals of 15 min. Aliquots (~6 μL) were delivered onto microscope slides using a pipet tip, trimmed to increase the opening diameter to ~1.5-mm, and imaged using the X100 objective on the LSM510 META laser scanning confocal microscope (Carl Zeiss, Thornwood, NY). Z-stacks are shown.

AUTHOR CONTRIBUTION

The experiments were designed and performed by Lili Zheng and James R. Bartles. Manuscript preparation and writing were performed by Lili Zheng, Stephen A. Adam, Jaime García-Anoveros and Brian J. Mitchell.

ACKNOWLEDGEMENTS

We want to thank Jonathan Bird and Jun Yang for generously providing reagents. Supported by grants R01 DC004314 (to JRB), R01 DC019834 (to JGA), R01 GM089970, (to BJM) from NIH.

CONFLICT OF INTEREST

The authors have no conflicts of interest.

DATA AVAILABILITY STATEMENT

The data that support the findings of this study are available from the corresponding author upon reasonable request.

REFERENCES

- Agrawal, Y., Carey, J. P., Della Santina, C. C., Schubert, M. C., & Minor, L. B. (2009). Disorders of balance and vestibular function in US adults: Data from the National Health and nutrition examination survey, 2001-2004. *Archives of Internal Medicine*, 169, 938-944. <https://doi.org/10.1001/archinternmed.2009.66>
- Bartles, J. R. (2000). Parallel Actin bundles and their multiple Actin-bundling proteins. *Current Opinion in Cell Biology*, 12, 72-78. [https://doi.org/10.1016/s0955-0674\(99\)00059-9](https://doi.org/10.1016/s0955-0674(99)00059-9)
- Bartles, J. R., Wierda, A., & Zheng, L. (1996). Identification and characterization of espin, an Actin-binding protein localized to the F-Actin-rich junctional plaques of Sertoli cell ectoplasmic specializations. *Journal of Cell Science*, 109(6), 1229-1239. <https://doi.org/10.1242/jcs.109.6.1229>

- Bartles, J. R., Zheng, L., Li, A., Wierda, A., & Chen, B. (1998). Small espin: A third Actin-bundling protein and potential forked protein ortholog in brush border microvilli. *The Journal of Cell Biology*, 143, 107–119. <https://doi.org/10.1083/jcb.143.1.107>
- Blackwell, D. L., Lucas, J. W., & Clarke, T. C. (2014). Summary health statistics for U.S. adults: National health interview survey, 2012. *Vital and Health Statistics*, 10, 1–161.
- Bock, G. R., & Steel, K. P. (1983). Inner ear pathology in the deafness mutant mouse. *Acta Oto-Laryngologica*, 96, 39–47. <https://doi.org/10.3109/00016488309132873>
- Boulouiz, R., Li, Y., Soualhia, H., Abidi, O., Chafik, A., Nürnberg, G., ... Barakat, A. (2008). A novel mutation in the Espin gene causes autosomal recessive nonsyndromic hearing loss but no apparent vestibular dysfunction in a Moroccan family. *American Journal of Medical Genetics. Part A*, 146a, 3086–3089. <https://doi.org/10.1002/ajmg.a.32525>
- Collins, F. L., Williams, J. O., Bloom, A. C., Stone, M. D., Choy, E., Wang, E. C., & Williams, A. S. (2015). Death receptor 3 (TNFRSF25) increases mineral apposition by osteoblasts and region specific new bone formation in the axial skeleton of male DBA/1 mice. *Journal of Immunology Research*, 2015, 901679. <https://doi.org/10.1155/2015/901679>
- Donaudy, F., Zheng, L., Ficarella, R., Ballana, E., Carella, M., Melchionda, S., ... Gasparini, P. (2006). Espin gene (ESPN) mutations associated with autosomal dominant hearing loss cause defects in microvillar elongation or organisation. *Journal of Medical Genetics*, 43, 157–161. <https://doi.org/10.1136/jmg.2005.032086>
- Drummond, I. A. (2012). Cilia functions in development. *Current Opinion in Cell Biology*, 24, 24–30. <https://doi.org/10.1016/j.ceb.2011.12.007>
- Fang, L., Adkins, B., Deyev, V., & Podack, E. R. (2008). Essential role of TNF receptor superfamily 25 (TNFRSF25) in the development of allergic lung inflammation. *The Journal of Experimental Medicine*, 205, 1037–1048. <https://doi.org/10.1084/jem.20072528>
- Fang, Q., Indzhukilian, A. A., Mustapha, M., Riordan, G. P., Dolan, D. F., Friedman, T. B., ... Bird, J. E. (2015). The 133-kDa N-terminal domain enables myosin 15 to maintain mechanotransducing stereocilia and is essential for hearing. *eLife*, 4. <https://doi.org/10.7554/eLife.08627>
- Grüneberg, H., Burnett, J. B., & Snell, G. D. (1941). The origin of jerker, a new gene mutation of the house mouse, and linkage studies made with it. *Proceedings of the National Academy of Sciences of the United States of America*, 27, 562–565. <https://doi.org/10.1073/pnas.27.12.562>
- Holme, R. H., Kiernan, B. W., Brown, S. D., & Steel, K. P. (2002). Elongation of hair cell stereocilia is defective in the mouse mutant whirler. *The Journal of Comparative Neurology*, 450, 94–102. <https://doi.org/10.1002/cne.10301>
- Kageyama, R., Shimojo, H., & Imayoshi, I. (2015). Dynamic expression and roles of Hes factors in neural development. *Cell and Tissue Research*, 359, 125–133. <https://doi.org/10.1007/s00441-014-1888-7>
- Krey, J. F., Krystofiak, E. S., Dumont, R. A., Vijayakumar, S., Choi, D., Rivero, F., ... Barr-Gillespie, P. G. (2016). Plastin 1 widens stereocilia by transforming Actin filament packing from hexagonal to liquid. *The Journal of Cell Biology*, 215, 467–482. <https://doi.org/10.1083/jcb.201606036>
- Krey, J. F., Wilmarth, P. A., David, L. L., & Barr-Gillespie, P. G. (2017). Analysis of the proteome of hair-cell Stereocilia by mass spectrometry. *Methods in Enzymology*, 585, 329–354. <https://doi.org/10.1016/bs.mie.2016.09.023>
- Loomis, P. A., Kelly, A. E., Zheng, L., Changyaleket, B., Sekerková, G., Mugnaini, E., ... Bartles, J. R. (2006). Targeted wild-type and jerker espins reveal a novel, WH2-domain-dependent way to make Actin bundles in cells. *Journal of Cell Science*, 119, 1655–1665. <https://doi.org/10.1242/jcs.02869>
- Mathur, P. D., Zou, J., Zheng, T., Almishaal, A., Wang, Y., Chen, Q., ... Yang, J. (2015). Distinct expression and function of whirlin isoforms in the inner ear and retina: An insight into pathogenesis of USH2D and DFNB31. *Human Molecular Genetics*, 24, 6213–6228. <https://doi.org/10.1093/hmg/ddv339>
- Mauriac, S. A., Hien, Y. E., Bird, J. E., Carvalho, S. D., Peyrourou, R., Lee, S. C., ... Montcouquiol, M. (2017). Defective Gpsm2/Gα (i3) signalling disrupts stereocilia development and growth cone Actin dynamics in Chudley-McCullough syndrome. *Nature Communications*, 8, 14907. <https://doi.org/10.1038/ncomms14907>
- Naz, S., Griffith, A. J., Riazuddin, S., Hampton, L. L., Battey, J. F., Jr., Khan, S. N., ... Friedman, T. B. (2004). Mutations of ESPN cause autosomal recessive deafness and vestibular dysfunction. *Journal of Medical Genetics*, 41, 591–595. <https://doi.org/10.1136/jmg.2004.018523>
- Neidt, E. M., Skau, C. T., & Kovar, D. R. (2008). The cytokinesis formins from the nematode worm and fission yeast differentially mediate Actin filament assembly. *The Journal of Biological Chemistry*, 283, 23872–23883. <https://doi.org/10.1074/jbc.M803734200>
- Orvis, J., Gottfried, B., Kancherla, J., Adkins, R. S., Song, Y., Dror, A. A., ... Hertzano, R. (2021). gEAR: Gene expression analysis resource portal for community-driven, multi-omic data exploration. *Nature Methods*, 18, 843–844. <https://doi.org/10.1038/s41592-021-01200-9>
- Perrin, B. J., Strandjord, D. M., Narayanan, P., Henderson, D. M., Johnson, K. R., & Ervasti, J. M. (2013). β-Actin and fascin-2 cooperate to maintain stereocilia length. *The Journal of Neuroscience*, 33, 8114–8121. <https://doi.org/10.1523/jneurosci.0238-13.2013>
- Probst, F. J., Fridell, R. A., Raphael, Y., Saunders, T. L., Wang, A., Liang, Y., ... Camper, S. A. (1998). Correction of deafness in shaker-2 mice by an unconventional myosin in a BAC transgene. *Science*, 280, 1444–1447. <https://doi.org/10.1126/science.280.5368.1444>
- Richardson, G. P., de Monvel, J. B., & Petit, C. (2011). How the genetics of deafness illuminates auditory physiology. *Annual Review of Physiology*, 73, 311–334. <https://doi.org/10.1146/annurev-physiol-012110-142228>
- Scheffer, D. I., Shen, J., Corey, D. P., & Chen, Z. Y. (2015). Gene expression by mouse inner ear hair cells during development. *The Journal of Neuroscience*, 35, 6366–6380. <https://doi.org/10.1523/jneurosci.5126-14.2015>
- Schreiber, T. H., & Podack, E. R. (2013). Immunobiology of TNFSF15 and TNFRSF25. *Immunologic Research*, 57, 3–11. <https://doi.org/10.1007/s12026-013-8465-0>
- Schreiber, T. H., Wolf, D., Boder, M., Gonzalez, L., & Podack, E. R. (2012). T cell costimulation by TNFR superfamily (TNFRSF)4 and TNFRSF25 in the context of vaccination. *Journal of Immunology*, 189, 3311–3318. <https://doi.org/10.4049/jimmunol.1200597>
- Schwander, M., Kachar, B., & Müller, U. (2010). Review series: The cell biology of hearing. *The Journal of Cell Biology*, 190, 9–20. <https://doi.org/10.1083/jcb.201001138>
- Sekerková, G., Richter, C. P., & Bartles, J. R. (2011). Roles of the espin Actin-bundling proteins in the morphogenesis and stabilization of hair cell stereocilia revealed in CBA/CaJ congenic jerker mice. *PLoS Genetics*, 7, e1002032. <https://doi.org/10.1371/journal.pgen.1002032>
- Sekerková, G., Zheng, L., Loomis, P. A., Changyaleket, B., Whitlon, D. S., Mugnaini, E., & Bartles, J. R. (2004). Espins are multifunctional Actin cytoskeletal regulatory proteins in the microvilli of chemosensory and mechanosensory cells. *The Journal of Neuroscience*, 24, 5445–5456. <https://doi.org/10.1523/jneurosci.1279-04.2004>
- Shin, J. B., Krey, J. F., Hassan, A., Metlagel, Z., Tauscher, A. N., Pagana, J. M., ... Barr-Gillespie, P. G. (2013). Molecular architecture of the chick vestibular hair bundle. *Nature Neuroscience*, 16, 365–374. <https://doi.org/10.1038/nn.3312>
- Tadenev, A. L. D., Akturk, A., Devanney, N., Mathur, P. D., Clark, A. M., Yang, J., & Tarchini, B. (2019). GPSM2-GNAI1 specifies the tallest Stereocilia and defines hair bundle row identity. *Current Biology*, 29, 921–934.e924. <https://doi.org/10.1016/j.cub.2019.01.051>
- Tilney, L. G., & DeRosier, D. J. (1986). Actin filaments, stereocilia, and hair cells of the bird cochlea. IV. How the Actin filaments become organized in developing stereocilia and in the cuticular plate.

- Developmental Biology*, 116, 119–129. [https://doi.org/10.1016/0012-1606\(86\)90048-5](https://doi.org/10.1016/0012-1606(86)90048-5)
- Vollrath, M. A., Kwan, K. Y., & Corey, D. P. (2007). The micromachinery of mechanotransduction in hair cells. *Annual Review of Neuroscience*, 30, 339–365. <https://doi.org/10.1146/annurev.neuro.29.051605.112917>
- Wiwatpanit, T., Lorenzen, S. M., Cantú, J. A., Foo, C. Z., Hogan, A. K., Márquez, F., ... García-Añoveros, J. (2018). Trans-differentiation of outer hair cells into inner hair cells in the absence of INSM1. *Nature*, 563, 691–695. <https://doi.org/10.1038/s41586-018-0570-8>
- Zampini, V., Rüttiger, L., Johnson, S. L., Franz, C., Furness, D. N., Waldhaus, J., ... Marcotti, W. (2011). Eps8 regulates hair bundle length and functional maturation of mammalian auditory hair cells. *PLoS Biology*, 9, e1001048. <https://doi.org/10.1371/journal.pbio.1001048>
- Zheng, J., Anderson, C. T., Miller, K. K., Cheatham, M., & Dallos, P. (2009). Identifying components of the hair-cell interactome involved in cochlear amplification. *BMC Genomics*, 10, 127. <https://doi.org/10.1186/1471-2164-10-127>
- Zheng, L., Beeler, D. M., & Bartles, J. R. (2014). Characterization and regulation of an additional Actin-filament-binding site in large isoforms of the stereocilia Actin-bundling protein espin. *Journal of Cell Science*, 127, 1306–1317. <https://doi.org/10.1242/jcs.143255>
- Zheng, L., Sekerková, G., Vranich, K., Tilney, L. G., Mugnaini, E., & Bartles, J. R. (2000). The deaf jerker mouse has a mutation in the gene encoding the espin Actin-bundling proteins of hair cell stereocilia and lacks espins. *Cell*, 102, 377–385. [https://doi.org/10.1016/s0092-8674\(00\)00042-8](https://doi.org/10.1016/s0092-8674(00)00042-8)

SUPPORTING INFORMATION

Additional supporting information can be found online in the Supporting Information section at the end of this article.

How to cite this article: Zheng, L., Adam, S. A., García-Añoveros, J., Mitchell, B. J., & Bartles, J. R. (2022). Espin overexpression causes stereocilia defects and provides an anti-capping effect on actin polymerization. *Cytoskeleton*, 79(6-8), 64–74. <https://doi.org/10.1002/cm.21719>